Non-contact biomimetic mechanism for selective hydrogenation of nitroaromatics on heterogeneous metal nanocatalysts

Wenting Zhou[1†], Laiyang Li[1†], Ruixuan Qin[1], Jiaxin Zhu[1], Shengjie Liu[1], Shiguang Mo[1], Zaifa Shi[1], Huihuang Fang[1], Pengpeng Ruan[1], Jun Cheng[1], Gang Fu[1*] & Nanfeng Zheng[1,2*]

[1]*State Key Laboratory for Physical Chemistry of Solid Surfaces, Collaborative Innovation Center of Chemistry for Energy Materials, and Department of Chemistry, College of Chemistry and Chemical Engineering, Xiamen University, Xiamen 361005, China;*
[2]*Innovation Laboratory for Sciences and Technologies of Energy Materials of Fujian Province (IKKEM), Xiamen 361005, China*

While the enzymatic reduction of unsaturated compounds usually has high specificity, highly selective reduction processes are hardly realized by heterogeneous industrial catalysts, which is critical for the green production of many fine chemicals. Here, we report an unexpected discovery of a biomimetic behavior of dicyandiamide (DICY)-modified Pt nanocatalysts for the green hydrogenation of a wide range of nitroaromatics. We demonstrate that the surface modification by DICY not only prevents the direct contact of nitroaromatic reactants with Pt surface but also induces an effective non-contact hydrogenation mechanism mediated by protons and electrons. In such a process, the DICY layer serves as a "semi-permeable membrane" to allow the permeation of H_2 molecules for being activated into electrons and protons at the Pt-DICY interface. With the generation of separated protons and electrons, the nitro group with strong electrophilic properties can be hydrogenated through the electron transfer followed by the proton transfer, which is facilitated by the hydrogen bonding network formed by protonated DICY. The unique mechanism makes it highly directional toward the hydrogenation of nitro groups without side reactions. Owing to its capability to largely eliminate the waste generation, the developed Pt-DICY catalysts have been successfully applied for the green industrial production of many important aniline intermediates.

hydrogenation catalysis, nitroaromatics, proton/electron separation, non-contact hydrogenation, biomimetic mechanism

1 Introduction

Catalytic hydrogenation plays a critical role in the manufacture of a very wide range of valuable chemicals [1–3]. For example, the selective hydrogenation of functional anilines from nitroaromatics is crucial for the production of pharmaceuticals, pesticides, dyes, perfumes, *etc*. To drive catalytic hydrogenation, the vital steps involve the activation of H_2 molecules followed by the transfer of the activated hydrogen species onto unsaturated bonds [4–6]. Heterolytic dissociation of H_2 into proton and hydride and homolytic dissociation into H atoms represent the two major activation pathways on metal-based catalysts [7–9]. Thus, in most hydrogenation reactions, reactants have to contact metal sites to pick up the activated hydrogen species, which can induce side reactions due to the undesired interaction between metal and reactants to be hydrogenated [10–12]. Spatially separating the reactants from the metal sites is an ideal solution to handle the issue. In fact, such non-contact mechanism is prevalent in bio-systems. For instance, the delicate micro-environment of hydrogenases [13] facilitates the activation

---

†These authors contributed equally to this work.
*Corresponding authors (email: nfzheng@xmu.edu.cn; gfu@xmu.edu.cn)

of H$_2$ to produce protons (H$^+$) and electrons (e$^-$) which are then transferred to reductases through the proton and electron channels to induce reduction reactions [14–19]. There has been a long-standing interest in synthetic catalysts to mimic the enzymatic hydrogenation processes by generating and utilizing H$^+$/e$^-$ pairs in a controllable manner [20–22]. Decorating metal catalysts with organic modifiers has been emerging as an effective strategy to mimic hydrogenases [23–25]. Although studies have demonstrated the capability of such a strategy to manipulate the interaction configuration of substances with the catalytic sites, no success has been reported on the identification of organic modifiers that can facilitate the activation of H$_2$ into H$^+$/e$^-$ pairs and direct those pairs for selective hydrogenation.

We report herein the successful fabrication of a biomimetic platinum-dicyandiamide (Pt-DICY) catalyst by modifying Pt nanocatalysts with a dense layer of DICY. The as-developed catalyst exhibits extremely high selectivity and activity in the hydrogenation of substituted nitroaromatics to anilines with alternating substituents (Figure S1, Supporting Information online). The systematic experiments and density functional theory (DFT) calculations reveal that the presence of heavily coated DICY blocks the direct contact of substituted nitroaromatics with Pt surface but still allows the adsorption and activation of H$_2$ into protons and electrons at the Pt-DICY interface. Even without direct contact with Pt surface, nitro groups are readily hydrogenated through a consecutive electron and proton transfer process, distinguishing from the existing contact hydrogenation mechanisms, such as Horiuti-Polanyi mechanism, H$^+$/H$^-$ hydrogenation mechanism and electrochemical (Haber) mechanism [6], but similar to the hydrogenation process in nitroreductase [26–28]. Such a unique catalytic mechanism prevents the side hydrogenations, making Pt-DICY an ideal platform for developing green hydrogenation processes for the industrial production of a wide range of functional anilines.

2 Results and discussion

2.1 Characterization and catalysis of DICY-modified Pt catalyst

In the present work, Pt nanocubes (Pt NCs) with major (100) exposing facet (Figure 1a) were synthesized [29]. DICY consisting of a guanido and a cyano group (Figure S2) was then introduced into an ethanol dispersion of Pt NCs, yielding the Pt NCs-DICY catalyst with well-defined Pt(100)-DICY interfaces. As revealed by the temperature-programmed desorption-mass spectrometric (TPD-MS) analysis, the Pt NCs-DICY catalyst displayed an obvious mass spectrometric signal of DICY at 360–480 °C (Figure S3), implying a rather strong interaction of DICY with Pt surface. Metal dispersion analysis (24.6% based on CO titration) and thermogravi-
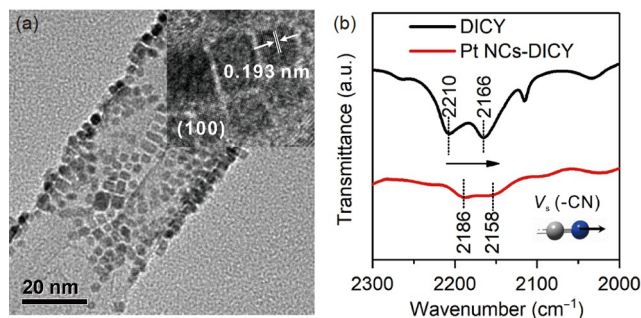

Figure 1 (a) Representative transmission electron microscope (TEM) images of Pt NCs with Pt(100) as the major exposure facets that were synthesized by reducing Pt(acac)$_2$ under CO. (b) Fourier-transform infrared (FTIR) spectra of DICY and Pt NCs-DICY in the region of 2,000–2,300 cm^{-1} (color online).

metric analysis (TGA) revealed that the ratio of the surface Pt atoms to the adsorbed DICY molecule was about 4:1 (Figure S4). As illustrated in the FTIR spectra (Figure 1b and Figure S5), compared with unbound DICY, adsorbed DICY displayed a vibrational red-shift from 2,210 (imino) and 2,166 (amino) to 2,186 and 2,158 cm^{-1} for the cyano group (–CN), indicating that both configurations of DICY would be retained upon adsorption and the anchoring points would be –CN groups with side-on mode [30–32].

The catalytic system of Pt NCs-DICY was then applied in the selective hydrogenation of *p*-chloronitrobenzene (*p*-CNB), a representative halogenated nitroaromatic compound. Similar to the commercial Pt/C catalyst, Pt NCs themselves suffered from serious dechlorination caused by the direct contact of aromatic ring with Pt surface and thus activation of C–Cl bonds (Figure 2a). While *p*-CNB was completely converted to *p*-chloroaniline (*p*-CAN) on Pt NCs within 20 min (Figure S6), nearly 10% by-product of aniline (AN) was produced. With the reaction time was elongated from 20 to 120 min, the selectivity of *p*-CAN was further decreased from 90% to 80%. In sharp contrast, the Pt NCs-DICY catalyst gave 100% conversion at ~60 min with a 99.5% selectivity to *p*-CAN even with the increased reaction time to 120 min. When the molar ratio of Pt to DICY was lower than 1, the yield of the side products, AN in the majority, was maintained at a very low level of 0.5% even with the prolonging reaction time beyond 6 h (Figures S7, S8). However, when nitriles or amines containing the same structural fragment of NH$_x$ as DICY were used as the additives (Figure 2b-I–V and Figure S9), the resulting catalysts did not exhibit a similar anti-dechlorination function to that of Pt NCs-DICY. And we also employed other organics as modifiers, including PPh$_3$, S=PPh$_3$, thiophene, and long chain thiols. In terms of activity and selectivity, DICY was still the best choice (Figure S10). These results clearly suggested that DICY and Pt should form a unique interface.

Previous works have demonstrated that the addition of some organic/inorganic blockers can deter dechlorination by
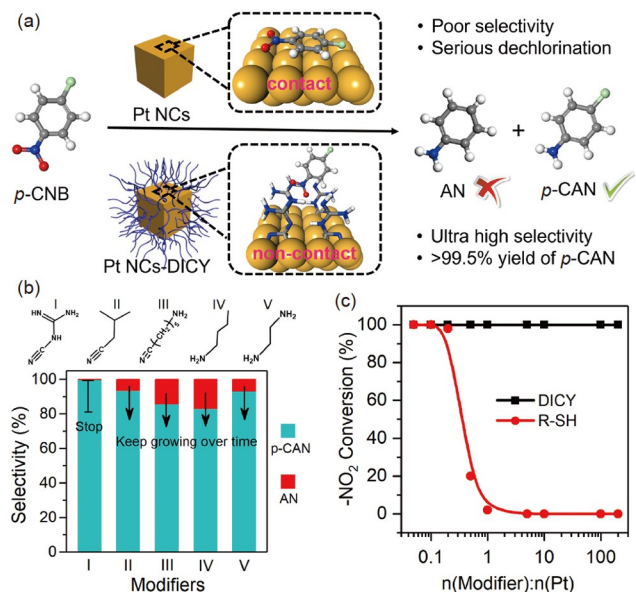
Figure 2 Catalytic performance of Pt-DICY interface. (a) Schematic illustration of the *p*-CNB hydrogenation in Pt NCs and Pt NCs-DICY (inset, the model of Pt NCs and Pt NCs-DICY). (b) *p*-CNB conversion and product distribution over DICY and other ligands-modified Pt NCs after reaction 2 h. The molar ratio was 1:1 for the Pt to all test organic additives. (c) The conversion of nitro group (–NO$_2$) after 2 h of *p*-CNB hydrogenation. The molar ratios of Pt and organic gradually increased from 1:0.05 to 1:200. R-SH: 1-octanethiol as representative (color online).

inhibiting the interaction of Ph-Cl with the metal surface [11,33,34]. However, in order to achieve the high *p*-CAN selectivity, introducing excess additives, such as 1-octanethiol, was often required. The catalytic activity would then sharply decay (Figure 2c and Figure S11). It was totally unexpected that the adding amount of DICY did not influence the –NO$_2$ conversion dramatically. Even with the increased *n*(DICY):*n*(Pt) ratio up to 200:1, the conversion of *p*-CNB to *p*-CAN was accomplished within 2 h (Figure S12a). Moreover, even in the hydrogenation of nitroaromatics having bulky substituents (*e.g.*, *tert*-butyl nitrobenzene, 1-chloro-2,5-dimethoxy-4-nitrobenzene, 5-chloro-2-nitrodiphenylamine), the use of high-concentration DICY did not inhibit the –NO$_2$ hydrogenation (Figure S12b–d). However, it was worth mentioning that the hindrance caused by the excessive addition of DICY will greatly inhibit the conversion of the –NHOH intermediate to –NH$_2$ (Figure S13). Taking into account all these findings, there should exist a unique noncontact mechanism behind the selective hydrogenation of *p*-CNB on Pt NCs-DICY to direct the reduction of –NO$_2$ only.

2.2 Proton-electron separation from H$_2$ occurring at Pt-DICY interface

To understand the unique function of DICY for *p*-CNB hydrogenation, we first explored the adsorption behavior of *p*-CNB on Pt NCs and Pt NCs-DICY. Experimentally, excess

p-CNB was introduced into the clean or DICY-modified Pt NCs, then washed carefully before IR characterization. As illustrated in Figure S14a, vibrational peaks of –NO$_2$ at 1,408 and 1,207 cm^{-1} were observed on the Pt NCs treated with *p*-CNB. However, no new peak associated with *p*-CNB was detected on the Pt NCs-DICY catalyst treated with *p*-CNB, confirming that the presence of DICY on Pt NCs blocked the Pt surface for the chemical adsorption of *p*-CNB so that direct interaction between Pt surface and *p*-CNB was inhibited. No adsorption of *p*-CNB on Pt NCs-DICY was also evidenced by TGA in which no additional weight loss was revealed on Pt NCs-DICY treated with *p*-CNB compared with that of Pt NCs-DICY (Figure S14b).

However, the surface DICY layer does not influence the adsorption-activation of H$_2$ on Pt NCs. Similar chemisorption capacities of H$_2$ were revealed on clean Pt NCs and DICY-modified Pt NCs (0.43 cm^3/g *vs.* 0.40 cm^3/g) (Figure S15). In addition, UV-Vis spectra showed that a similar amount of DICY was adsorbed on Pt NCs-DICY before and after the treatment of H$_2$ (Figure S16). IR spectra revealed the interaction of adsorbed DICY with H species activated on Pt. While two distinct bands at 2,158 and 2,186 cm^{-1} corresponding to the –CN groups in the conjugated imino and amino were observed on the Pt NCs-DICY catalyst under Ar atmosphere [35], only single peak at 2,058 cm^{-1} for the conjugated bonds was revealed on the catalyst under H$_2$ flow (Figure 3a). Moreover, the signal attributed to –NH$_x$ at 3,140 cm^{-1} was enhanced (Figure 3c), which was more significant under D$_2$ atmosphere (–ND$_x$ at 2,357 cm^{-1}) [36]. Control experiment demonstrated that in the absence of Pt NCs, the structure of pure DICY did not change upon the introduction of H$_2$ (Figure 3b). Taking all these data together, we speculated that part of dissociated H species was transferred from Pt surface to DICY and adsorbed thereon.

One should note that upon H$_2$ treatment, the IR red-shift of –CN bond on Pt-DICY was still in the vibrational range of –C≡N bond rather than –C=N or –C–N. Such a red shift was thus ascribed to the electronic structure change of the Pt surface upon introducing H$_2$. CO was adopted as a probe to further confirm the electronic change with the introduction of H$_2$. As shown in Figure 3d, while CO adsorption with typical atop and bridge configurations (at 2,072 and 1,872 cm^{-1}) was observed on Pt NCs, no chemisorption of CO was observed on Pt NCs-DICY under Ar. However, the introduction of H$_2$ dramatically changed the CO chemisorption behavior on Pt NCs-DICY with the appearance of obvious atop (2,021 cm^{-1}) and bridge (1,849 cm^{-1}) adsorption bands. In comparison, no obvious vibration shift of CO was observed on unmodified Pt NCs with H$_2$ treatment. Typically, CO prefers to adsorb more strongly on the electron-rich Pt surface than that with Pt$^{\delta+}$. The hardly detected CO binding on Pt NCs-DICY might be explained by the generation of the Pt$^{\delta+}$ surface due to the electron withdrawing
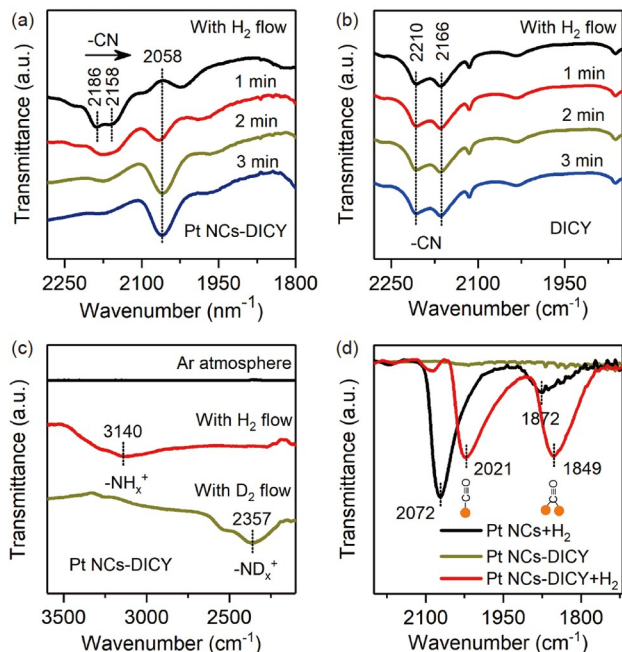
Figure 3 The evolution of H_2 at the Pt-DICY interface. (a) IR spectra of Pt NCs-DICY under H_2 treatment. (b) IR spectra of DICY under H_2 treatment. (c) IR difference spectra of Pt NCs-DICY under Ar, H_2 and D_2 atmosphere. The results were measured after Ar purge. The spectrum of Pt NCs-DICY was recorded and used as background. (d) *In situ* DRIFTS study of CO adsorption on Pt NCs and Pt NCs-DICY. Pt NCs and Pt NCs-DICY were pretreated with 30 mL/min H_2 at 60 °C before CO adsorption (color online).

by a large amount of DICY molecules bound on the surface. When H_2 was introduced onto Pt NCs-DICY, the proton-electron separation led to the migration of a large number of protons to the DICY layer and also the generation of electron-rich Pt surface. Such an electron-rich Pt surface would back donate more electrons to CO than the normal Pt(0) surface, nicely explaining why the CO adsorption on Pt NCs-DICY displayed a red shift relative to that on Pt NCs. All these results came to the conclusion that H_2 molecules were activated into electrons and protons at the Pt NCs-DICY interface.

Based on the above experimental characterizations, a structural model was built to simulate the Pt NCs-DICY catalyst in which four DICY molecules were adsorbed on the four-fold hollow sites through the –CN group within a (4×4) Pt(100) slab. According to DFT calculations, the most stable adsorption pattern for DICY molecules on Pt contained half DICY molecules in amino configuration and half in imino, and two distinct bands at 2,158 and 2,186 cm^{-1} in the IR spectrum do corroborate our theoretical model with the formation of amino-imino pairs, due to the formation of favorable hydrogen-bonding among them (Figure S17). Computationally, the parallel adsorption of *p*-CNB on clean Pt (structure A in Figure S18) was by far the most stable, while the perpendicular adsorption of *p*-CNB through the –NO$_2$ group had not much difference on clean Pt (structure B) and Pt-DICY (structure C). To our surprise, H_2 was readily

dissociated homogeneously into H atoms on exposing Pt atoms by surmounting a barrier of 0.45 eV without destroying the coordinative configuration of the pre-adsorbed DICY (Figure S19). Once the H atoms formed, the proton-coupled electron transfer process between the Pt surface and guanido in DICY readily took place *via* a seven-membered ring transition state (TS1 and TS1') by overcoming barriers of 1.10 and 0.74 eV, respectively (Figures S20, S21). Interestingly, the protonated DICY would undergo tautomerization in which proton transfer from guanidyl to cyan group occurred by passing a small barrier of 0.09 eV (TS2) or 0.29 eV (TS2'). The guanido group would then seize another proton from Pt surface by overcoming barriers of 0.91 eV (TS3) and 0.55 eV (TS3'), respectively. From the viewpoint of thermodynamics, totally 14 H atoms (8 H on Pt and 6H on DICY) at the Pt-DICY interface would reach the energy minimum (Figure S22). Moreover, we found that the transfer of protons between different DICY molecules was calculated to be viable with small barriers of 0.10–0.46 eV (Figure S23). It should be noted that the NanoSelect catalysts, HHDMA-modified Pt, developed by BASF, also displayed very high selectivity for the reduction of substituted nitroaromatics. However, DICY and HHDMA are chemically very different: (1) DICY is a small organic base with one anchoring site (cyan group) and relatively small van der Waals contributions; (2) in contrast to HHDMA, higher DICY content results in slightly lower reactivity but significantly enhanced selectivity; (3) DICY can pick up protons from surface and serve as proton sponge [37,38].

The next question needed to be addressed was where the electrons were located after the proton transfer. Figure 4 illustrates the differential Bader charge of the Pt DICYs system upon H_2 dissociation, which was referenced to the clean Pt-DICYs. Our DFT calculations showed that the first four H_2 molecules would be dissociated into H atoms which were still situated on Pt. Only a slight charge separation between the surface and organic layers was observed during this process. In contrast, when three more H_2 molecules approached the interface to yield 6 pairs of H^+/e^-, the organic layer became more positively charged (+1.13 a.u.) while the surface and subsurface Pt carried more negative charge (−1.13 a.u.). It should be pointed out that electrons and protons are not able to be completely separated at the interface as the electrons would be redistributed accompanying the uptake of protons so that part of electrons would store on the organic layer.

2.3   Non-contact hydrogenation mechanism at Pt-DICY interface

To understand why Pt-DICY catalyst can conduct the directional hydrogenation of *p*-CNB, we further investigated the hydrogenation mechanism. As shown in Figure S24, the
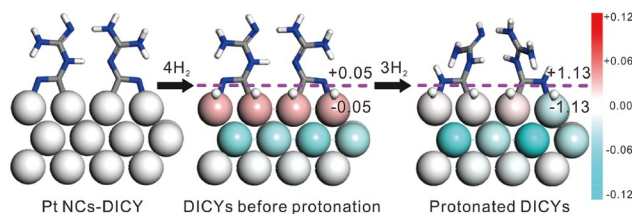
Figure 4　Differential Bader charge of the hydrogenated Pt-DICYs as referenced with the clean Pt-DICYs. In order to illustrate the charge separation, the interface is roughly divided into surface layers and organic layer (color online).

–NO$_2$ group in *p*-CNB can interact with the protonated DICY with the adsorption energy of −1.01 eV (VII), which is far stronger than the typical H-bond interaction. Bader charge analysis showed that *p*-CNB had acquired 0.48 electrons upon adsorption. Thus, the strong adsorption can be rationalized in terms of the Columbic interaction between *p*-CNB anion and protonated DICY layer. Figure 5b plotted the Bader charge and the adsorption energy of *p*-CNB against the distance of the N atom of –NO$_2$ and Pt surface. It was clear to see that when *p*-CNB was placed far away from the Pt surface, *i.e.*, 10 Å, the molecule nearly kept neutral and the adsorption energy was predicted to be −0.10 eV. With *p*-CNB approaching the surface, the *p*-CNB gained more negative charge, and the adsorption energy went down steadily, indicating that the electron transfer would readily occur. However, we were not able to locate the proton transfer TS starting from VII despite our best effort. Alternatively, we located a metastable intermediate (VIII) by moving an H atom from cyano to guanidinyl group. Such a state is 0.46 eV less favorable than VII, but the *p*-CNB thereon hold more negative charge (−0.80 a.u.) as compared with that on VII. Interestingly, VIII reacts easily with a proton at DICY layer by overcoming a small barrier of 0.12 eV (TS4), creating a free radical in such a way that electron transfer promotes proton transfer. Then the resulting radical dehydrated to form *p*-CNsB through H transfer *via* TS5. This step involves a barrier of 0.17 eV with an exothermicity of 0.72 eV (Figure 5a and Figure S25). To further confirm the non-contact hydrogenation mechanism, we also performed the Carr-Parrinello molecular dynamics, as shown in Figure 5c and Figure S26. It was clear to see that the first and the second O–H bonds would be formed at 1.7 and 5.7 ps, respectively, indicating that the separated H$^+$/e$^−$ pairs at Pt-DICY interface directs the hydrogenation on O of –NO$_2$ group. Interestingly, such a hydrogenation mechanism at the Pt-DICY interface was similar to the –NO$_2$ reduction in nitroreductase [27], in which the flavin mononucleotide (FMN) cofactor played a similar role as DICY (Figure 6) [39–41]. Based on these discussions, we inferred that the hydrogenation barrier should critically depend on the degree of protonation on DICY. Experimentally, within the tested pressure in the range of 1–5 bar, the H$_2$ reaction order was 0.7 for Pt NCS-DICY,
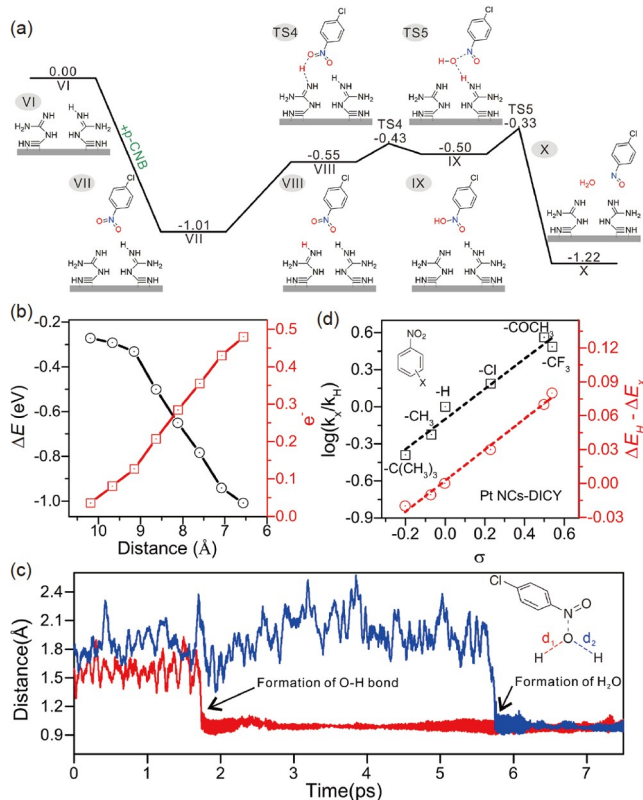

Figure 5　Unique mechanism for the reduction of –NO$_2$ to –NO over DICY layer. (a) Reaction profile and models of intermediates and transition states in the –NO$_2$ hydrogenation. (b) The electron transfers from Pt-DICY to *p*-CNB. It is clear that the shorter the distance between *p*-CNB and Pt surface, the stronger the adsorption energy and the more negative charge accumulating in *p*-CNB. (c) The variation of O–H bond during the hydrogenation of –NO$_2$ simulating by the Carr-Parrinello molecular dynamics (CPMD). The CPMD calculation starts from the structure of VIII at 330 K and the timestep is set to 0.5 fs. (d) Hammett plot and differential barriers for the X-Ph-NO$_2$ (X = 4-CF$_3$, 4-COCH$_3$, 4-Cl, 4-H, 3-CH$_3$, 4-C(CH$_3$)$_3$) hydrogenation against the σ parameter. The differential barrier was defined as the energy difference of the effective barrier (VII→TS5) between the substituted nitrobenzene and nitrobenzene (color online).

distinguished from Pt NCs (0.3) (Figure S27).

To gain deeper insight on the non-contact hydrogenation process, we also explored the hydrogenation kinetics of a series of para-substituted nitrobenzenes (X-Ph-NO$_2$, where X was CF$_3$, C(O)CH$_3$, Cl + F, Cl, H, CH$_3$, CHO or C(CH$_3$)$_3$) using Pt NCs-DICY as the catalyst. As shown in Figure S28a and Table S2 (Supporting Information online), there existed a positive correlation between hydrogenation rate and the electron withdrawing ability of the substituent group. A Hammett plot against σ revealed a linear relationship with a positive slope (ρ = 1.22; Figure 5d). This observation suggested a buildup of negative charge on the nitrobenzene unit in the transition state (TS). The rate-determining step should thus be the process of negative charge accumulation [42]. Bader charge analysis showed that more and more negative charges would accumulate on *p*-CNB unit along the hydrogenation, increasing from −0.48 a.u. in VI to −1.47 a.u. in X, c.f. Figure S29. According to DFT calculations, the effective
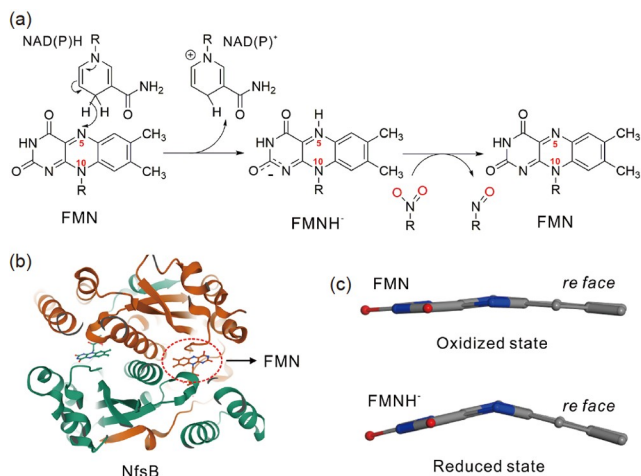
Figure 6 (a) The catalytic mechanism of nitroreductase NfsB in –NO$_2$ hydrogenation. The –NO$_2$ hydrogenation in nitroreductase NfsB was mediated by the redox cofactor FMN [27]. At first, the NAD(P)H delivered protons and electrons to FMN to produce FMNH$^-$, and then the RNO$_2$ would be reduced by getting the protons and electrons from reduced FMNH$^-$. (b) Crystal structure of *Escherichiacoli* nitroreductase NfsB mutant T41L/N71S/F124W [39]. (c) The conformational change of FMN during the redox process [40,41] (color online).

barrier (VII→TS5) can correlate well with σ (Figure S30 and Table S1). In sharp contrast to Pt NCs-DICY, the hydrogenation rate of R-Ph-NO$_2$ in Pt NCs was not correlated well with the substituent constant (σ) (Figures S28b and S31) because the steric effect would also be taken into consideration, accounting for low hydrogenation activity for the bulky substituent, such as C(CH$_3$)$_3$ (Figure S28c).

Once –NO$_2$ was hydrodeoxygenated, the intermediates, such as –NO (*p*-chloronitrosobenzene, *p*-CNsB) and –NHOH (*p*-chlorophenylhydroxylamine, *p*-CPOA) (Figure S32), were readily reacted with Pt surface by replacing DICY on Pt due to the strong binding capability of their nitrogen sites. The hydrogenation of these species should then compete with the adsorption of DICY. It is thus not surprising that the –NHOH intermediates were accumulated during the hydrogenation process. During the hydrogenation from *p*-CNsB to *p*-CPOA to *p*-CAN, the interaction between the N binding sites and Pt surface is the main factor to determine the reaction rate as well as to effectively prevent the C–Cl bonds from being activated and hydrogenated to induce dechlorination. In addition to halogen, the hydroxyl, methoxyl and methyl groups were well maintained during the hydrogenation of –NO$_2$. By adopting the non-contact mechanism disclosed in this work, many green hydrogenation processes have now been already utilized in the industry (Table 1).

3 Conclusions

In summary, we have successfully developed a biomimetic

Table 1 Chemoselective hydrogenation of different substituted nitroarenes over commercial 2 wt% Pt/C catalysts modified by DICY[a]

Entry	Substrate	Sel. (%)
1	3-Cl	99
2	3-Br	98.9
3	4-Br	99.7
4	3-I	>99
5	4-I	96
6	4-F	>99
7	4-CF$_3$	>99
8	2-CF$_3$	97
9	4-C(CH$_3$)$_3$	99.6
10	4-COCH$_3$	99.3
11	4-H	>99
12	4-Cl, 2-F	98.6
13	4-CHO	98.7
14	4-CH$_3$	98
15	3-CH$_3$	99.8
16	2,3-Cl	99.3/99.8*
17	3,4-Cl	99.5/99.5*
18	2,5-Cl	>99/99.9*
19	3-Cl,6-OH	98.7/99.5*
20	2-CH$_3$, 3-Cl	>99/99.6*
21	2,4-CH$_3$, 5-Cl	97.1/99.5*
22	2,5-OCH$_3$, 4-Cl	99*
23	3-OCH(OCH$_3$)$_2$, 4,6-Cl	>99*
24	4-Cl, 2-NHPh	98.5

a) Reaction conditions: T = 60 °C, P = 1 bar, Pt/substrate = 1/400, 1 mmol substrate, n(Pt):n(DICY) = 1:200, 10 mL ethanol as solvent, concentration measured by normalized peak area in high performance liquid chromatography (HPLC) or gas chromatography (GC). * Data from the industry process adopting the technology developed in this work. The annual production capacity of Entries 18, 19, 20, 22, 23 and *p*-CAN was 20,000, 500, 5,000, 2,000, 1,500 and 2,000 tons, respectively.

heterogeneous Pt catalyst that enables the activation of H$_2$ into proton/electron pairs to display an extremely high selectivity and activity in the hydrogenation of a wide range of substituted nitroaromatics to high-purity anilines, without the occurrence of other side reactions to generate undesired by-products. The key to the process is to modify Pt nanocatalysts with a dense layer of dicyandiamide containing coordinating groups as well as rich proton binding sites of –NH$_2$, =NH, =N–. The dicyandiamide layer serves as "semipermeable membrane" to allow the permeation of H$_2$ molecules for being activated into electrons and protons at the Pt-DICY interface, but prevent the direct contact of nitroaromatics with the Pt surface. The most important contribution of this work lies in the discovery of a non-contact nitroreductase-like mechanism that nicely illustrates how proton/electron pairs can be effectively utilized for the selective hydrogenation of nitro groups. Such a non-contact mechanism secures the extremely high selectivity toward the hy-

drogenation of only nitro groups on nitroaromatics since the aromatic rings are always away from the Pt surface during the hydrogenation. The importance of this work is further enhanced by the successful application of the non-contact mechanism for the green industrial productions of a wide spectrum of functional anilines from nitroaromatics. The enzyme-like heterogeneous hydrogenation process demonstrated in this work not only provides a new avenue for industrial hydrogenations but also helps to bridge the gap between enzymatic catalysis and heterogeneous catalysis.

Conflict of interest   The authors declare no conflict of interest.

Supporting information   The supporting information is available online at http://chem.scichina.com and http://link.springer.com/journal/11426. The supporting materials are published as submitted, without typesetting or editing. The responsibility for scientific accuracy and content remains entirely with the authors.

1 Graciani J, Mudiyanselage K, Xu F, Baber AE, Evans J, Senanayake SD, Stacchiola DJ, Liu P, Hrbek J, Fernández Sanz J, Rodriguez JA. *Science*, 2014, 345: 546–550

2 Kyriakou G, Boucher MB, Jewell AD, Lewis EA, Lawton TJ, Baber AE, Tierney HL, Flytzani-Stephanopoulos M, Sykes ECH. *Science*, 2012, 335: 1209–1212

3 Corma A, Serna P. *Science*, 2006, 313: 332–334

4 Chai Y, Wu G, Liu X, Ren Y, Dai W, Wang C, Xie Z, Guan N, Li L. *J Am Chem Soc*, 2019, 141: 9920–9927

5 Aich P, Wei H, Basan B, Kropf AJ, Schweitzer NM, Marshall CL, Miller JT, Meyer R. *J Phys Chem C*, 2015, 119: 18140–18148

6 Fiorio JL, López N, Rossi LM. *ACS Catal*, 2017, 7: 2973–2980

7 García-Melchor M, López N. *J Phys Chem C*, 2014, 118: 10921–10926

8 Sellmann D, Prakash R, Heinemann FW, Moll M, Klimowicz M. *Angew Chem Int Ed*, 2004, 43: 1877–1880

9 Taylor MJ, Durndell LJ, Isaacs MA, Parlett CMA, Wilson K, Lee AF, Kyriakou G. *Appl Catal B-Environ*, 2016, 180: 580–585

10 Marshall ST, O'Brien M, Oetter B, Corpuz A, Richards RM, Schwartz DK, Medlin JW. *Nat Mater*, 2010, 9: 853–858

11 Makosch M, Lin WI, Bumbálek V, Sá J, Medlin JW, Hungerbühler K, van Bokhoven JA. *ACS Catal*, 2012, 2: 2079–2081

12 Albani D, Vilé G, Mitchell S, Witte PT, Almora-Barrios N, Verel R, López N, Pérez-Ramírez J. *Catal Sci Technol*, 2016, 6: 1621–1631

13 Kuchenreuther JM, Guo Y, Wang H, Myers WK, George SJ, Boyke CA, Yoda Y, Alp EE, Zhao J, Britt RD, Swartz JR, Cramer SP. *Biochemistry*, 2013, 52: 818–826

14 Vincent KA, Li X, Blanford CF, Belsey NA, Weiner JH, Armstrong FA. *Nat Chem Biol*, 2007, 3: 761–762

15 Frey M. *ChemBioChem*, 2002, 3: 153–160

16 Schilter D, Camara JM, Huynh MT, Hammes-Schiffer S, Rauchfuss TB. *Chem Rev*, 2016, 116: 8693–8749

17 Tai H, Hirota S, Stripp ST. *Acc Chem Res*, 2021, 54: 232–241

18 Peters JW, Schut GJ, Boyd ES, Mulder DW, Shepard EM, Broderick JB, King PW, Adams MWW. *BioChim Biophys Acta (BBA) - Mol Cell Res*, 2015, 1853: 1350–1369

19 Huang G, Wagner T, Ermler U, Shima S. *Nat Rev Chem*, 2020, 4: 213–221

20 Slocik JM, Govorov AO, Naik RR. *Angew Chem Int Ed*, 2008, 47: 5335–5339

21 Meeuwissen J, Reek JNH. *Nat Chem*, 2010, 2: 615–621

22 Manea F, Houillon FB, Pasquato L, Scrimin P. *Angew Chem Int Ed*, 2004, 43: 6165–6169

23 Reback ML, Ginovska-Pangovska B, Ho MH, Jain A, Squier TC, Raugei S, Roberts JAS, Shaw WJ. *Chem Eur J*, 2013, 19: 1928–1941

24 Simmons TR, Berggren G, Bacchi M, Fontecave M, Artero V. *Coord Chem Rev*, 2014, 270-271: 127–150

25 Zaffaroni R, Detz RJ, van der Vlugt JI, Reek JNH. *ChemSusChem*, 2018, 11: 209–218

26 Hannink N, Rosser SJ, French CE, Basran A, Murray JAH, Nicklin S, Bruce NC. *Nat Biotechnol*, 2001, 19: 1168–1172

27 Race PR, Lovering AL, Green RM, Ossor A, White SA, Searle PF, Wrighton CJ, Hyde EI. *J Biol Chem*, 2005, 280: 13256–13264

28 Lovering AL, Hyde EI, Searle PF, White SA. *J Mol Biol*, 2001, 309: 203–213

29 Chen G, Tan Y, Wu B, Fu G, Zheng N. *Chem Commun*, 2012, 48: 2758–2760

30 Sexton BA, Avery NR. *Surf Sci*, 1983, 129: 21–36

31 Shayeghi A, Krähling S, Hörtz P, Johnston RL, Heard CJ, Schäfer R. *J Phys Chem C*, 2017, 121: 21354–21363

32 Adamczyk AJ. *Surf Sci*, 2019, 682: 84–98

33 Kahsar KR, Schwartz DK, Medlin JW. *J Am Chem Soc*, 2014, 136: 520–526

34 Vilé G, Almora-Barrios N, López N, Pérez-Ramírez J. *ACS Catal*, 2015, 5: 3767–3778

35 Xu KX, Guo MH, Ren LQ, Huang W, Sun JJ. *Sci China Chem*, 2018, 61: 360–367

36 Collado JA, Ramírez FJ. *J Raman Spectrosc*, 1999, 30: 391–397

37 Yezhelyev MV, Qi L, O'Regan RM, Nie S, Gao X. *J Am Chem Soc*, 2008, 130: 9006–9012

38 Belding L, Stoyanov P, Dudding T. *J Org Chem*, 2016, 81: 553–558

39 Bai J, Zhou Y, Chen Q, Yang Q, Yang J. *ChemBioChem*, 2015, 16: 1219–1225

40 Haynes CA, Koder RL, Miller AF, Rodgers DW. *J Biol Chem*, 2002, 277: 11513–11520

41 Hecht HJ, Erdmann H, Park HJ, Sprinzl M, Schmid RD. *Nat Struct Mol Biol*, 1995, 2: 1109–1114

42 Chalkley MJ, Garrido-Barros P, Peters JC. *Science*, 2020, 369: 850–854